ACS Energy LETTERS

http://pubs.acs.org/journal/aelccp

LETTER

Grain Transformation and Degradation Mechanism of Formamidinium and Cesium Lead Iodide Perovskite under Humidity and Light

Kevin Ho, Mingyang Wei, Edward H. Sargent, and Gilbert C. Walker*

Cite This: *ACS Energy Lett.* 2021, 6, 934–940

Read Online

ACCESS | Metrics & More | Article Recommendations | Supporting Information

ABSTRACT: Mixed cation perovskites have improved stability, but cation alloying enables the formation of separated phases, as well as leading to new decomposition pathways. Here, using photothermal infrared microscopy, we report degradation mechanisms in $FA_{0.85}Cs_{0.15}PbI_3$, a study enabled by our ability to resolve the location of formamidinium (FA) cations with <100 nm spatial resolution. We find that upon exposure to either light or water alone, no decomposition nor change in the spatial distribution of FA was observed. However, upon exposure to both light and high humidity simultaneously, $FA_{0.85}Cs_{0.15}PbI_3$ degrades through a multistep pathway within 30 h. First, the $FA_{0.85}Cs_{0.15}PbI_3$ phase separates to δ_o-$CsPbI_3$, δ-$FAPbI_3$, and PbI_2 and the spatial distribution of FA becomes increasingly heterogeneous. Second, FA evaporates from δ-$FAPbI_3$ and PbI_2 remained. Understanding the degradation pathways will aid in the design of more stable perovskites with, for example, the suppressing of grain transformation during the phase separation.

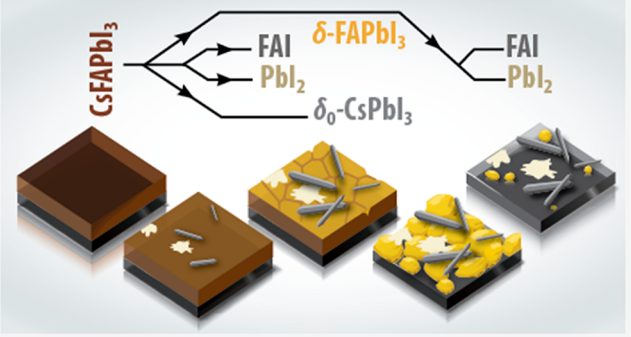

Lead halide perovskites have achieved a high power conversion efficiency and are promising candidates for future solar cells due to high absorption coefficients, long carrier diffusion lengths, and ease of fabrication.[1−3] One major challenge yet to be fully overcome is instability to factors such as moderate heat, light, and water.[4−8]

To make a more stable perovskite, different cations and anions have been combined. For example, cations such as methylammonium (MA), formamidinium (FA), or Cs and halides such as iodine or bromine have frequently been mixed.[9] Although mixed ion perovskites provide better stability than single ion perovskites, phase separation into pure perovskite phases can occur. For example, halide segregation is known to be detrimental to properties.[10−15] Cation migration and phase separation have been significantly less studied.[16−19]

In addition to phase separation, degradation of mixed cation perovskites under different environmental factors such as light and humidity is also less well understood. Specifically, the dependence among these factors has not been thoroughly investigated.

In particular, the degradation mechanism of perovskite grains and the growth of impurities have not been well characterized on the length scales of individual grains. Prior studies have relied mainly on power conversion efficiency, UV/vis absorption, X-ray diffraction (XRD), and scanning electron microscopy (SEM),[20] but these lack the spatial resolution and direct chemical identification to probe compositional changes within grains vs boundaries. It is known that humidity degradation starts from the grain boundaries and is highly sensitive to the boundary chemistry and grain size.[21−23] In addition, grain boundaries have been shown to affect the optoelectronic properties of the perovskite.[24−26] We reasoned that developing a deeper understanding of how the individual grains change structurally and chemically during the degradation or phase separation could assist in further development of even more stable perovskites.

In this work, we study the grains individually, witnessing chemical and structural changes during the light and humidity-

Received: October 21, 2020
Accepted: December 23, 2020

https://dx.doi.org/10.1021/acsenergylett.0c02247
ACS Energy Lett. 2021, 6, 934–940

induced degradation of mixed cation perovskites. To accomplish this, we focus on the photothermal induced resonance (PTIR) to image the organic component of the perovskites. PTIR[27] couples atomic force microscopy (AFM) and vibrational spectroscopy and enables vibrational absorption imaging at a spatial resolution of <100 nm[27] (Figure 2a), in contrast to conventional Fourier transform infrared spectroscopy (FTIR) with ~3 μm spatial resolution. Because of this, the PTIR signal can be related to specific organic components (e.g., FA), in contrast to other AFM based techniques such as conductance AFM or Kelvin probe force microscopy (KPFM). PTIR has been used to characterize perovskites, but they have not been used to track the complete phase separation and decomposition pathways of the different grain types.[28−32]

To demonstrate the validity of PTIR, both PTIR and FTIR spectra were collected on a $FA_{0.85}Cs_{0.15}PbI_3$/ITO sample (Figure S1). This cation ratio has been favored among FA and Cs mixed perovskites.[33,34] The intense formamidinium C═N stretch at 1712 cm^{-1} appears in both PTIR and the infrared spectra, which can be used for the unambiguous identification of the FA cation.

Degradation with Humidity and/or Light. Next, we use AFM and PTIR to study the light and humidity degradation of mixed cation perovskites. The perovskite structure $FA_{0.85}Cs_{0.15}PbI_3$/ITO/glass was exposed to three different light and relative humidity (RH) conditions: (i) high humidity in the dark, (ii) high humidity under light, and (iii) low humidity under light. High (low) humidity and light degradations were performed at 85% RH (20% RH) and a 10 mW/cm^2 light source. The spectra of the light source and the absorption spectra of the fresh perovskite are shown in Figure 1. Changes in the adhesion as RH increases suggest that water is adsorbed onto the perovskite surface (Figure S2).

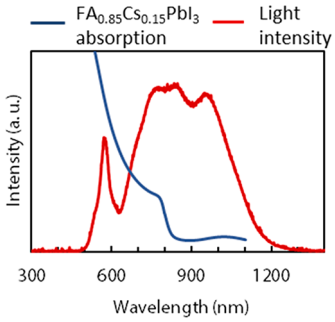

Figure 1. Spectrum of the light source used for illumination and absorption spectra of the fresh perovskite.

We observed that in cases i and iii, the morphology and PTIR intensity did not change (Figure 2b,d; complete set of data in Figures S3 and S4), consistent with previous studies that have shown no decay in perovskites in storage (dark) conditions within 20 h.[33] In addition, PTIR images do not show a large variation in the signal intensity before and after exposure, in comparison with case ii. This suggests that the distribution of the FA ions does not change after exposure to light or humidity alone. Although PTIR can be used to track the distribution of the FA cation, it cannot distinguish between the α and δ phases of $FAPbI_3$. For this, we turned to XRD (Figures S3 and S4) and found that no phase transformation occurred during these times. The similarity in morphology and PTIR before and after of cases i and iii also shows that the experimental setup does not induce degradation to the perovskites. For further explanation, refer to Supporting Information.

In contrast to cases i and iii, large heterogeneous grains are observed in case ii, in contrast to the smooth homogeneous film in the fresh sample when exposed to both high humidity and light. Second, some grains show an increase in the PTIR intensity while others have lost intensity, indicating that the FA distributions have changed.

To determine if FA in case ii decays through different pathways or if it is just an accelerated version of cases i and iii, the degradations have been carried out for an extended time (>100 h) (Figure S5). We found that depressions formed for case iii at longer times but were not observed for case i; instead, large grains started to form at high RH and extended exposure times. This suggests that the degradation pathway is different for light or high RH and will be further discussed below.

Next, we focus on the AFM and PTIR images collected in shorter intervals to probe the degradation pathways upon exposure to both light and water simultaneously (case ii, Figure 3). Complete set of data in Figures S6 and S7). In addition, XRD, time-of-flight secondary ion mass spectrometry (TOF-SIMS), UV/vis, and photoluminescence (PL) were measured to identify the inorganic components and different crystal phases. In-situ imaging was not carried out due to possible degradation that can be caused by the AFM and PTIR setup (see Supporting Information).

Degradation with Light and Humidity Simultaneously: 0−7 h. In the fresh film, no clear inhomogeneity of the PTIR intensity was observed (Figure 3a), suggesting that FA was uniformly distributed. The sample homogeneity was further confirmed by the TOF-SIMS FA, Cs, Pb, and I maps (Figure 4a). In XRD, signature peaks at 2θ = 13.7, 19.6, 24.0, 27.9, and 31.3° show that α-$FA_{0.85}Cs_{0.15}PbI_3$ dominates at 0 h (Figure 4b).[17] UV/vis and PL spectra (Figure 4d) show an absorption/emission edge at ~800 nm, typical of the perovskite. After 5 h of exposure to light and high RH, depressions and needles begin to develop, as seen in the AFM topography. However, the grain size and inhomogeneity of the PTIR intensity do not show any significant change for the remainder of the sample. A significant increase in the PL spectra after illuminating for 2 h was attributed to lattice distortion and trap elimination leading to an enhancement in PL.[35]

Depressions. PTIR images (Figure 3b) and spectra (Figure S8) at 1712 cm^{-1} on the depressions show a reduced absorption compared to the fresh sample. Furthermore, the lack of additional peaks from 1500 to 1800 cm^{-1} suggest that the depressions do not contain FA and are instead inorganic. In TOF-SIMS (Figure 4a), the Pb map outlines the depressions (indicated by the arrow) and shows a distinct signal from the surrounding grains. Zoomed-out TOF-SIMS and AFM images are used to better identify the depressions (Figure S9). Note that the TOF-SIMS signal cannot be directly related to the concentration of the materials since the ionization properties can be different in different environments.[36] In addition, TOF-SIMS samples the top 1−2 nm of the perovskite, which may not be representative of the bulk.[36] With the above information, we identify the material in the bottom of the depressions as PbI_2. This is also evident in the XRD spectra at 6 h with a peak for PbI_2 at 2θ = 12.5° (Figure 4b). The formation of PbI_2 accompanied by the formation of

https://dx.doi.org/10.1021/acsenergylett.0c02247
ACS Energy Lett. 2021, 6, 934−940

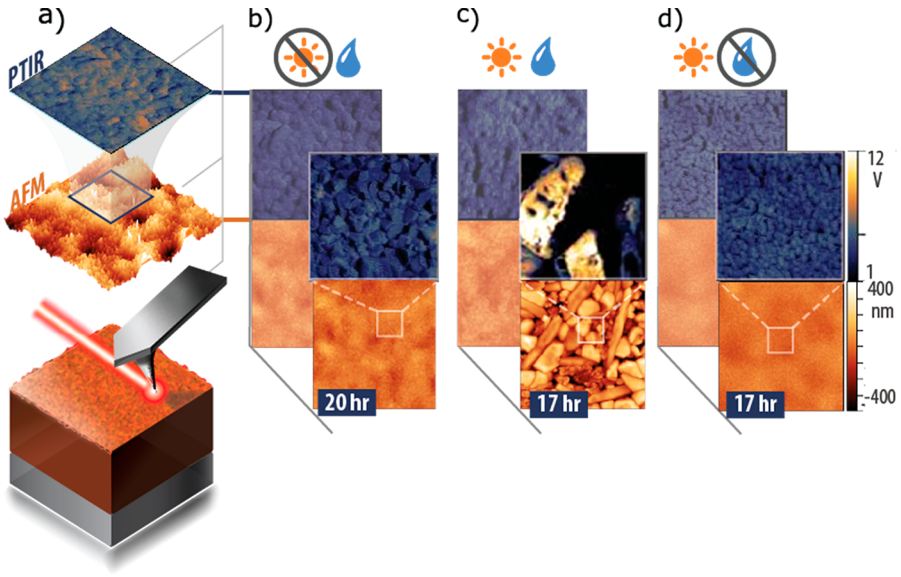

Figure 2. (a) Schematic showing AFM and PTIR images obtained on the same area. (b)−(d) PTIR imaging at 1712 cm^{-1} (top, blue) and AFM morphology (bottom, orange) showing the change between the fresh sample (back panel) and after exposure (front panel). (b) High humidity in the dark (case i). (c) High humidity under light (case ii). (d) Low humidity under light (case iii). The PTIR images are 2 × 2 μm^2 and the AFM height images are 10 × 10 μm^2.

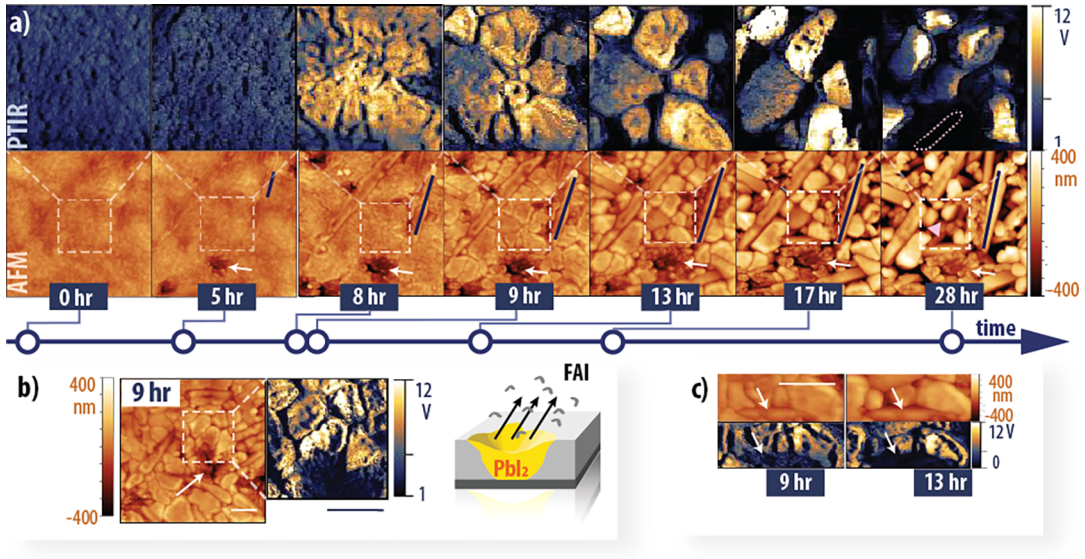

Figure 3. (a) AFM morphology (orange) and PTIR (blue) at 1712 cm^{-1} showing the changing morphology and spatially inhomogeneous IR absorption when exposed to high humidity and light (case ii, Figure 2c). The AFM images are 10 × 10 μm^2, and the PTIR images are 4 × 4 μm^2 measured in the areas indicated by the white dashed squares. The white arrows show the depressions, and the blue lines in the AFM images follow a needle. The pink triangle in the AFM height and the dashed outline in the PTIR image indicate the small needle after the large grain shrinks. (b) AFM and PTIR image showing no absorption at 1712 cm^{-1} in the valley. The scale bars are 2 μm. The schematic shows FAI evaporates, and depressions form. (c) AFM and PTIR image of the needle, the scale bar is 2 μm, and the scales are the same for all images in (c). The arrows indicate the position of the needle.

volatile formamidinium iodide (FAI) explains why the depressions form in the film.[37−39] Solid-state FAI was not observed in the film due to the absence of PTIR peaks at 1600 and 1695 cm^{-1} (Figure S8).

The formation of depressions was also observed for extended exposure to light at low RH, but at a much slower rate (Figure S5). However, the depressions were not observed even after 100 h in the dark. Therefore, the formation of depression must be photoinduced but catalyzed by high RH.

Needles. Like the depressions, the needles also lack a peak at 1712 cm^{-1} for both PTIR images (Figure 3c) and spectra (Figure S8), suggesting that the needles are purely inorganic. In TOF-SIMS, the needles are characterized by the strong Cs and I intensity (220 au), while these signals are lower elsewhere. Note that the Cs and I maps show different areas since different experimental setup was used to obtain the cation (Cs, FA, Pb) and anion (I) maps. The needles are most likely orthorhombic (δ_o) $CsPbI_3$. In the XRD spectra, small peaks corresponding to δ_o-$CsPbI_3$ (2θ = 10°) appeared after 6 h. The low intensity of these peaks may be due to the small fraction of Cs originally present in the sample

https://dx.doi.org/10.1021/acsenergylett.0c02247
ACS Energy Lett. 2021, 6, 934−940

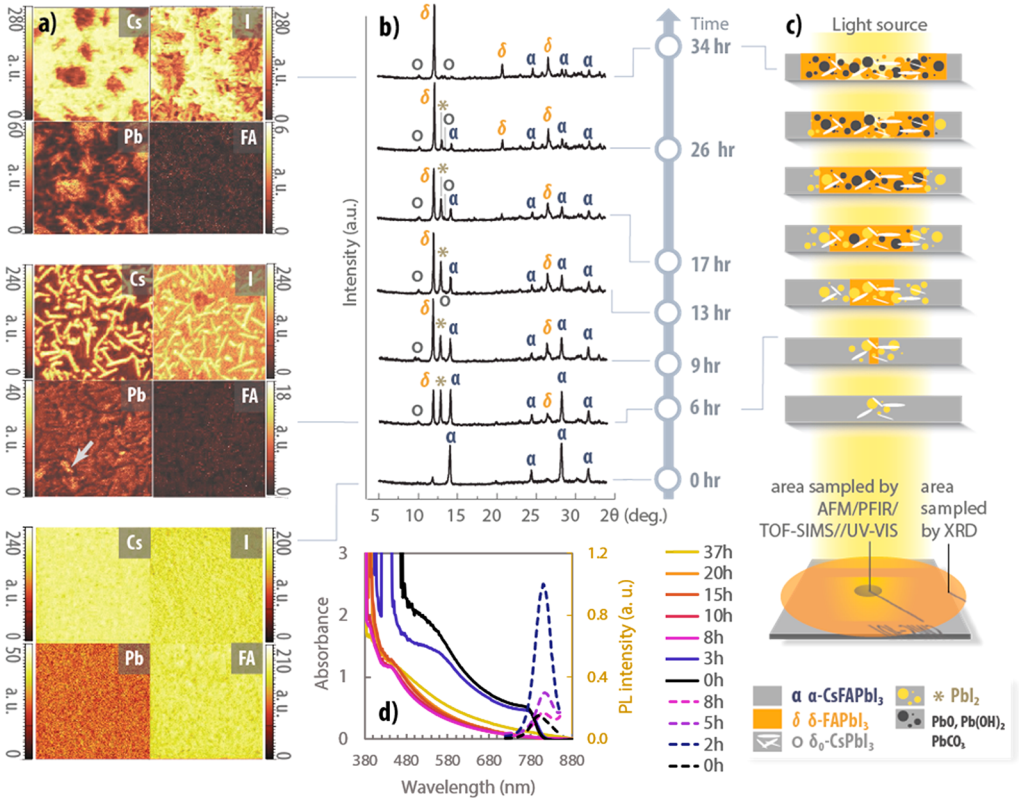

Figure 4. (a) TOF-SIMS of Cs^+, I^-, Pb^+, and FA ($CN_2H_5^+$) at 0, 6, and 34 h. All images are 20 × 20 μm^2. (b) XRD at different degradation times. (c) Schematic showing how the degradation proceeds. (d) UV/vis absorption and PL spectra of the degradation.

($FA_{0.85}Cs_{0.15}PbI_3$). Furthermore, the peak at ~440 nm in the UV/vis absorption spectra corresponds to the δ_o-$CsPbI_3$.[40]

Degradation with Light and Humidity Simultaneously: 8−11 h. From 8 to 11 h, the small grains in the fresh sample rapidly merged into larger grains in the AFM topography. PTIR intensity rapidly increased in parts of the film and large variations in PTIR intensity were observed (Figure 3a). To confirm that the changes in PTIR signal are not instrumental artifacts, PTIR images were collected at 1800 cm^{-1}, a nonabsorbing wavenumber, and no PTIR signal contrast was observed (Figure S11).

The large change in PTIR and AFM maps can be explained by the formation of δ-$FAPbI_3$ as the large grains. The increase of PTIR signal is due to the higher concentration of FA in δ-$FAPbI_3$ in comparison with $FA_{0.85}Cs_{0.15}PbI_3$. The exclusion of $CsPbI_3$ also allowed larger and smoother grains of phase pure δ-$FAPbI_3$ to form. In XRD, the δ-$FAPbI_3$ peak at 2θ = 11.5° appeared after 6 h and continues to grow for longer times. In addition, the peak at 390 nm in the UV/vis spectra also corresponds to δ-$FAPbI_3$.[33] In the TOF-SIMS image, the FA signal decreased drastically from 0 to 6 h. The TOF-SIMS signal is strongly dependent on the chemical environment and is only sensitive to the top surface layer while PTIR penetrates a few hundred nanometers. It is likely that δ-$FAPbI_3$ would have a lower FA signal in comparison to α-$FA_{0.85}Cs_{0.15}PbI_3$ since the δ phase is more stable than the mixed perovskite phase. Therefore, it may be possible that δ-$FAPbI_3$ has started to form on the top layer, which results in the low TOF-SIMS signal.

In contrast to the perovskite phase, δ-$FAPbI_3$ and δ_o-$CsPbI_3$ are structurally incompatible.[41] Therefore, as $FA_{0.85}Cs_{0.15}PbI_3$ undergoes phase transformation to the more stable δ phase, phase separation into δ-$FAPbI_3$ and δ_o-$CsPbI_3$ (needles) naturally follows.

Perovskite exposure to light is known to induce halide migration through the separation of holes and electron pairs and through the electric field generated.[42] This process can be possible for the cation, although happening at a much slower time scale.[16,18,19] Migration of cations would create Cs or FA rich regions, which would make the local energy of mixing unfavorable and thus lead to a demixing of $CsPbI_3$ and $FAPbI_3$ pure phases.[18] In addition, the local unbalance of Cs and FA concentrations can be caused by the depressions that initiate a cascade of phase separation and further degradations.

Exposure to high RH in the dark also shows the formation of large grains after 85 h. It has been reported that water can create larger grains in perovskites.[32] It may also be possible these are the start of the δ phase formation. Hydrogen bonding of perovskite with water has been found to disrupt the ionic bonding in the perovskite lattice and lowers the energy barrier for the degradation.[37] This process can also be responsible for mixed cation perovskite phase separation and explains why the depressions formation and further degradation happen at a higher rate at high RH.

Degradation with Light and Humidity Simultaneously: 11−13 h. From 11 to 13 h, almost no change of the morphology or increase in area was observed. This can be seen in the AFM roughness vs time plot (Figure S12) where at 11−13 h a plateau in roughness increase is seen. To further quantify the degradation, the areas of each material (depressions, needles, and grains) from Figure 3 are plotted as a function of time (Figure S13a−c). The two-step growth process is clearly visible, where at 11−13 h, the smooth growth curve is discontinued. Furthermore, the growth kinetics of FAI, $CsPbI_3$,

https://dx.doi.org/10.1021/acsenergylett.0c02247
ACS Energy Lett. 2021, 6, 934−940

and PbI_2 were modeled using the Johnson−Mehl−Avrami−Kolmogorov (JMAK) equation (Figure S13d−f) in order to determine the growth rate constant and the dimensionality of growth, which were found to be drastically different before and after 13 h.

Degradation with Light and Humidity Simultaneously: 13−34 h. From 13−28 h, the large grains shrink and are replaced by smaller needles that do not absorb at 1712 cm^{-1} (Figure 3a, pink triangle and dashed outline). Consequently, the averaged AFM roughness and PTIR intensity decreased (Figure S12). In addition, the average film thickness decreased from 690 to 490 nm as the grains disappear (Figure S14), suggesting that as the large grains convert to small needles, a volatile component leaves the material.

From 13 to 28 h, the PTIR intensity varied strongly among grains and within individual grains. PTIR point spectra at two different grains were taken at different degradation times (Figure S15). We found that the peak intensity, position, and width changes drastically as the grains shrink. This may be due to the change of interactions of the formamidinium cation C═N bond with other adjacent ions such as water or iodide,[32,37] possibly due to intermediate complexes with water or iodide formed during the liberation of volatile FAI.[37] Previous studies have suggested that hydrogen bonding between FA and water disrupt the bonding between FA and I in the lattice and allows the FA to become volatile.[37] However, further studies are needed to understand the exact mechanism of this degradation at the molecular level.

In XRD, the δ-$FAPbI_3$ peak increased from 17 to 34 h, which may seem contradictory with the shrinking δ-$FAPbI_3$ grains in PTIR. However, in PTIR we sampled the illuminated areas of 4 × 4 μm^2, but the XRD signals are averaged over the whole wafer. It is likely that in the small area sampled by AFM, PTIR, and TOF-SIMS, δ-$FAPbI_3$ has already degraded, but δ-$FAPbI_3$ continues to grow until it covers the whole light expose area (Figure 4c). With very long exposure to light and humidity, it is expected that all the δ-$FAPbI_3$ will decompose to FAI and PbI_2.

When the large grains shrink with the evaporation of FAI, the small needles that remain are most likely PbI_2. In TOF-SIMS, the Pb signal is most intense in the depressions but also present in the small needles. However, in XRD, the PbI_2 peak gradually disappeared from 17 to 34 h (Figure 4b), suggesting that PbI_2 further decomposed. PbI_2 has been reported to decompose into metallic lead Pb^0 and I_2 with light[38,43] or lead salts such as PbO, $Pb(OH)_2$, or $PbCO_3$ in humid air.[44−46] Using X-ray photoelectron spectroscopy (XPS), we found additional O and C 1s peaks and shift in the Pb 4f peaks (Figure S17). However, Pb^0 peaks were not observed. This suggests that oxygen containing lead salts such as PbO, $Pb(OH)_2$, or $PbCO_3$ are formed at long degradation times (see the Supporting Information for more information). PbI_2 can originate from two sources: (i) the material in the bottoms of depressions and (ii) the small needles. The amount of PbI_2 at a given time is determined by how fast the perovskite decomposes into PbI_2 and how fast PbI_2 decomposes further.

In the TOF-SIMS images, Cs and I signal increased, which likely is due to more inorganic components such as $CsPbI_3$ revealed when the large grains shrink. In addition, Cs and I typically have a very strong signal since these elements are very easily ionized. It has been reported that $CsPbI_3$ can photodecompose into CsI and PbI_2;[47,48] thus, it is possible that some needles are CsI.

Degradation of Another Composition of $FA_xCs_{1-x}PbI_3$. In addition to $FA_{0.85}Cs_{0.15}PbI_3$, we have also investigated the degradation of $FA_{0.70}Cs_{0.30}PbI_3$ and $FA_{0.95}Cs_{0.05}PbI_3$ to understand the effect of FA and Cs compositions on the degradation. We observed similar morphological changes using AFM (Figure S18). However, the first phase separation step occurs faster for both $FA_{0.70}Cs_{0.30}PbI_3$ and $FA_{0.95}Cs_{0.05}PbI_3$ than $FA_{0.85}Cs_{0.15}PbI_3$. This is consistent with the result that $FA_{0.85}Cs_{0.15}PbI_3$ has the lowest energy of mixing.[18] In addition, the amounts of needles formed increases with the amount of Cs concentration since the needles are δ_o-$CsPbI_3$.

In conclusion, we have demonstrated that the degradation is accelerated under simultaneous exposure to light and high RH. With light at low RH, depressions also formed but at a much slower rate; consequently, similar subsequent degradation is expected but at a reduced rate. However, with high RH in the dark, depressions are not formed but instead large grains developed after 80 h of exposure. Thus, the degradation probably occurs through a different pathway. Under light and high RH, the degradation occurs through the following pathway. At the first stage of degradation, 0−11 h, depressions (PbI_2) are formed as FAI evaporates. The mixed cation perovskite, $FA_{0.85}Cs_{0.15}PbI_3$ phase separates into needles (δ_o-$CsPbI_3$) and large grains (δ-$FAPbI_3$). At 11−13 h, the degradation stops. After 13 h, the second stage of degradation starts, with the large grains (δ-$FAPbI_3$) shrinking as FAI evaporates and more PbI_2 remains which can decay further. Degradation studies on this perovskite systems have been reported.[18,49] However, in this work, we relate the decomposition products to the grain types, providing the microstructure images of degradation process. We also studied the degradation under different stressors and revealed the accelerated degradation under both light and high humidity to relate the decomposition products to the grain types.

Although this report focuses only on $FA_xCs_{1-x}PbI_3$, these findings provide insights to the degradation of other mixed cation systems containing FA and Cs. Understanding the degradation pathway can lead to designing a more stable mixed cation perovskites device, for example, using additives or adlayers that prevent the early depression formation or inhibit the rapid grain growth that occurs during the α to δ phase transformation.

■ ASSOCIATED CONTENT

Supporting Information

The Supporting Information is available free of charge at https://pubs.acs.org/doi/10.1021/acsenergylett.0c02247.

Experimental methods and materials, comparison of PTIR and FTIR, adhesion vs RH, control experiments for PTIR, AFM at extended degradation times, full data set for AFM and PTIR degradation, PTIR of needles and depressions, additional comments on possible error source, AFM roughness and PTIR intensity changes over time, changes to area of material types over time and kinetics of degradation, PTIR spectra at different times, changes of film thickness during degradation, photographs of film during degradation, XPS spectra, degradation of $FA_xCs_{1-x}PbI_3$ with various composition x (PDF)

https://dx.doi.org/10.1021/acsenergylett.0c02247
ACS Energy Lett. 2021, 6, 934−940

AUTHOR INFORMATION

Corresponding Author

Gilbert C. Walker − *Department of Chemistry, University of Toronto, Toronto, Ontario M5S 3H6, Canada;* orcid.org/0000-0002-5248-5498; Email: gilbert.walker@utoronto.ca; thewalkerlab.com

Authors

Kevin Ho − *Department of Chemistry, University of Toronto, Toronto, Ontario M5S 3H6, Canada;* orcid.org/0000-0003-2688-2606

Mingyang Wei − *Department of Electrical and Computer Engineering, University of Toronto, Toronto, Ontario M5S 1A4, Canada*

Edward H. Sargent − *Department of Electrical and Computer Engineering, University of Toronto, Toronto, Ontario M5S 1A4, Canada;* orcid.org/0000-0003-0396-6495

Complete contact information is available at: https://pubs.acs.org/10.1021/acsenergylett.0c02247

Notes

The authors declare no competing financial interest.

ACKNOWLEDGMENTS

Funding for this work was supported by the Natural Science and Engineering Research Council of Canada (NSERC) and Canadian Foundation for Innovation (CFI). The authors acknowledge Peter M. Brodersen at the Ontario Centre for the Characterization of Advanced Materials (OCCAM), funded by the Canadian Foundation for Innovation and the Ontario Research Fund, for providing us with TOF-SIMS and XPS data. The authors thank Prof. Chih-Shan Tan for helpful discussions, and Dr. Joseph Manion for reading over the manuscript and providing comments.

REFERENCES

(1) Jena, A. K.; Kulkarni, A.; Miyasaka, T. Halide Perovskite Photovoltaics: Background, Status, and Future Prospects. *Chem. Rev.* **2019**, *119* (5), 3036−3103.

(2) Green, M. A.; Ho-Baillie, A. Perovskite Solar Cells: The Birth of a New Era in Photovoltaics. *ACS Energy Lett.* **2017**, *2* (4), 822−830.

(3) Qiu, L.; He, S.; Ono, L. K.; Liu, S.; Qi, Y. Scalable Fabrication of Metal Halide Perovskite Solar Cells and Modules. *ACS Energy Lett.* **2019**, *4* (9), 2147−2167.

(4) Boyd, C. C.; Cheacharoen, R.; Leijtens, T.; McGehee, M. D. Understanding Degradation Mechanisms and Improving Stability of Perovskite Photovoltaics. *Chem. Rev.* **2019**, *119* (5), 3418−3451.

(5) Christians, J. A.; Habisreutinger, S. N.; Berry, J. J.; Luther, J. M. Stability in Perovskite Photovoltaics: A Paradigm for Newfangled Technologies. *ACS Energy Lett.* **2018**, *3* (9), 2136−2143.

(6) Senocrate, A.; Kim, G. Y.; Grätzel, M.; Maier, J. Thermochemical Stability of Hybrid Halide Perovskites. *ACS Energy Lett.* **2019**, *4* (12), 2859−2870.

(7) Fransishyn, K. M.; Kundu, S.; Kelly, T. L. Elucidating the Failure Mechanisms of Perovskite Solar Cells in Humid Environments Using In Situ Grazing-Incidence Wide-Angle X-Ray Scattering. *ACS Energy Lett.* **2018**, *3* (9), 2127−2133.

(8) Yang, J.; Siempelkamp, B. D.; Liu, D.; Kelly, T. L. Investigation of $CH_3NH_3PbI_3$ Degradation Rates and Mechanisms in Controlled Humidity Environments Using *in Situ* Techniques. *ACS Nano* **2015**, *9* (2), 1955−1963.

(9) Ono, L. K.; Juarez-Perez, E. J.; Qi, Y. Progress on Perovskite Materials and Solar Cells with Mixed Cations and Halide Anions. *ACS Appl. Mater. Interfaces* **2017**, *9* (36), 30197−30246.

(10) Yoon, S. J.; Kuno, M.; Kamat, P. V. *Shift Happens*. How Halide Ion Defects Influence Photoinduced Segregation in Mixed Halide Perovskites. *ACS Energy Lett.* **2017**, *2* (7), 1507−1514.

(11) Elmelund, T.; Seger, B.; Kuno, M.; Kamat, P. V. How Interplay between Photo and Thermal Activation Dictates Halide Ion Segregation in Mixed Halide Perovskites. *ACS Energy Lett.* **2020**, *5* (1), 56−63.

(12) Braly, I. L.; Stoddard, R. J.; Rajagopal, A.; Uhl, A. R.; Katahara, J. K.; Jen, A. K.-Y.; Hillhouse, H. W. Current-Induced Phase Segregation in Mixed Halide Hybrid Perovskites and Its Impact on Two-Terminal Tandem Solar Cell Design. *ACS Energy Lett.* **2017**, *2* (8), 1841−1847.

(13) Elmelund, T.; Scheidt, R. A.; Seger, B.; Kamat, P. V. Bidirectional Halide Ion Exchange in Paired Lead Halide Perovskite Films with Thermal Activation. *ACS Energy Lett.* **2019**, *4* (8), 1961−1969.

(14) Huang, Z.; Proppe, A. H.; Tan, H.; Saidaminov, M. I.; Tan, F.; Mei, A.; Tan, C.-S.; Wei, M.; Hou, Y.; Han, H.; Kelley, S. O.; Sargent, E. H. Suppressed Ion Migration in Reduced-Dimensional Perovskites Improves Operating Stability. *ACS Energy Lett.* **2019**, *4* (7), 1521−1527.

(15) Hoke, E. T.; Slotcavage, D. J.; Dohner, E. R.; Bowring, A. R.; Karunadasa, H. I.; McGehee, M. D. Reversible Photo-Induced Trap Formation in Mixed-Halide Hybrid Perovskites for Photovoltaics. *Chem. Sci.* **2015**, *6* (1), 613−617.

(16) Domanski, K.; Roose, B.; Matsui, T.; Saliba, M.; Turren-Cruz, S.-H.; Correa-Baena, J.-P.; Carmona, C. R.; Richardson, G.; Foster, J. M.; De Angelis, F.; et al. Migration of Cations Induces Reversible Performance Losses over Day/Night Cycling in Perovskite Solar Cells. *Energy Environ. Sci.* **2017**, *10* (2), 604−613.

(17) Limpamanoch, P.; Rujisamphan, N.; Kumnorkaew, P.; Amornkitbamrung, V.; Tang, I.-M.; Zhang, Q.; Supasai, T. Understanding Effects of Cesium in $CH(NH_2)_2PbI_3$ for Stabilizing $CH(NH_2)_2PbI_3$ /$CsPbI_3$ Interface under UV Illumination. *J. Phys. Chem. C* **2019**, *123* (19), 12117−12125.

(18) Schelhas, L. T.; Li, Z.; Christians, J. A.; Goyal, A.; Kairys, P.; Harvey, S. P.; Kim, D. H.; Stone, K. H.; Luther, J. M.; Zhu, K.; Stevanovic, V.; Berry, J. J. Insights into Operational Stability and Processing of Halide Perovskite Active Layers. *Energy Environ. Sci.* **2019**, *12* (4), 1341−1348.

(19) Pavlovetc, I. M.; Brennan, M. C.; Draguta, S.; Ruth, A.; Moot, T.; Christians, J. A.; Aleshire, K.; Harvey, S. P.; Toso, S.; Nanayakkara, S. U.; Messinger, J.; Luther, J. M.; Kuno, M. Suppressing Cation Migration in Triple-Cation Lead Halide Perovskites. *ACS Energy Lett.* **2020**, *5*, 2802−2810.

(20) Rahman, M. Z.; Edvinsson, T. X-Ray Diffraction and Raman Spectroscopy for Lead Halide Perovskites. In *Characterization Techniques for Perovskite Solar Cell Materials*; Elsevier: 2020; pp 23−47.

(21) Castro-Méndez, A.; Hidalgo, J.; Correa-Baena, J. The Role of Grain Boundaries in Perovskite Solar Cells. *Adv. Energy Mater.* **2019**, *9* (38), 1901489.

(22) Yun, J. S.; Kim, J.; Young, T.; Patterson, R. J.; Kim, D.; Seidel, J.; Lim, S.; Green, M. A.; Huang, S.; Ho-Baillie, A. Humidity-Induced Degradation via Grain Boundaries of $HC(NH_2)_2PbI_3$ Planar Perovskite Solar Cells. *Adv. Funct. Mater.* **2018**, *28* (11), 1705363.

(23) Meggiolaro, D.; Mosconi, E.; De Angelis, F. Formation of Surface Defects Dominates Ion Migration in Lead-Halide Perovskites. *ACS Energy Lett.* **2019**, *4* (3), 779−785.

(24) Jiang, X.; Hoffman, J.; Stoumpos, C. C.; Kanatzidis, M. G.; Harel, E. Transient Sub-Band-Gap States at Grain Boundaries of $CH_3NH_3PbI_3$ Perovskite Act as Fast Temperature Relaxation Centers. *ACS Energy Lett.* **2019**, *4* (7), 1741−1747.

(25) Giridharagopal, R.; Precht, J. T.; Jariwala, S.; Collins, L.; Jesse, S.; Kalinin, S. V.; Ginger, D. S. Time-Resolved Electrical Scanning Probe Microscopy of Layered Perovskites Reveals Spatial Variations in Photoinduced Ionic and Electronic Carrier Motion. *ACS Nano* **2019**, *13* (3), 2812−2821.

(26) Li, Y.; Sun, W.; Gu, F.; Ouyang, D.; Bian, Z.; Liu, Z.; Choy, W. C. H.; Kelly, T. L. Soldering Grain Boundaries Yields Inverted Perovskite Solar Cells with Enhanced Open-Circuit Voltages. *Adv. Mater. Interfaces* **2019**, *6* (14), 1900474.
(27) Wang, L.; Wang, H.; Wagner, M.; Yan, Y.; Jakob, D. S.; Xu, X. G. Nanoscale Simultaneous Chemical and Mechanical Imaging via Peak Force Infrared Microscopy. *Sci. Adv.* **2017**, *3* (6), No. e1700255.
(28) Chae, J.; Dong, Q.; Huang, J.; Centrone, A. Chloride Incorporation Process in $CH_3NH_3PbI_{3-x}Cl_x$ Perovskites via Nanoscale Bandgap Maps. *Nano Lett.* **2015**, *15* (12), 8114−8121.
(29) Chatterjee, R.; Pavlovetc, I. M.; Aleshire, K.; Hartland, G. V.; Kuno, M. Subdiffraction Infrared Imaging of Mixed Cation Perovskites: Probing Local Cation Heterogeneities. *ACS Energy Letters* **2018**, *3* (2), 469−475.
(30) Yu, H. M.; Oh, H. M.; Park, D. Y.; Jeong, M. S. Nanochemical Investigation of Degradation in Organic−Inorganic Hybrid Perovskite Films Using Infrared Nanoscopy. *J. Phys. Chem. C* **2020**, *124* (6), 3915−3922.
(31) Szostak, R.; Silva, J. C.; Turren-Cruz, S.-H.; Soares, M. M.; Freitas, R. O.; Hagfeldt, A.; Tolentino, H. C. N.; Nogueira, A. F. Nanoscale Mapping of Chemical Composition in Organic-Inorganic Hybrid Perovskite Films. *Sci. Adv.* **2019**, *5* (10), No. eaaw6619.
(32) Nishida, J.; Alfaifi, A. H.; Gray, T. P.; Shaheen, S. E.; Raschke, M. B. Heterogeneous Cation−Lattice Interaction and Dynamics in Triple-Cation Perovskites Revealed by Infrared Vibrational Nanoscopy. *ACS Energy Lett.* **2020**, *5* (5), 1636−1643.
(33) Li, Z.; Yang, M.; Park, J.-S.; Wei, S.-H.; Berry, J. J.; Zhu, K. Stabilizing Perovskite Structures by Tuning Tolerance Factor: Formation of Formamidinium and Cesium Lead Iodide Solid-State Alloys. *Chem. Mater.* **2016**, *28* (1), 284−292.
(34) Lee, J.-W.; Kim, D.-H.; Kim, H.-S.; Seo, S.-W.; Cho, S. M.; Park, N.-G. Formamidinium and Cesium Hybridization for Photo- and Moisture-Stable Perovskite Solar Cell. *Adv. Energy Mater.* **2015**, *5* (20), 1501310.
(35) Kim, H.; Hagfeldt, A. Photoinduced Lattice Symmetry Enhancement in Mixed Hybrid Perovskites and Its Beneficial Effect on the Recombination Behavior. *Adv. Opt. Mater.* **2019**, *7* (9), 1801512.
(36) Harvey, S. P.; Li, Z.; Christians, J. A.; Zhu, K.; Luther, J. M.; Berry, J. J. Probing Perovskite Inhomogeneity beyond the Surface: TOF-SIMS Analysis of Halide Perovskite Photovoltaic Devices. *ACS Appl. Mater. Interfaces* **2018**, *10* (34), 28541−28552.
(37) Smecca, E.; Numata, Y.; Deretzis, I.; Pellegrino, G.; Boninelli, S.; Miyasaka, T.; La Magna, A.; Alberti, A. Stability of Solution-Processed $MAPbI_3$ and $FAPbI_3$ Layers. *Phys. Chem. Chem. Phys.* **2016**, *18* (19), 13413−13422.
(38) Juarez-Perez, E. J.; Ono, L. K.; Maeda, M.; Jiang, Y.; Hawash, Z.; Qi, Y. Photodecomposition and Thermal Decomposition in Methylammonium Halide Lead Perovskites and Inferred Design Principles to Increase Photovoltaic Device Stability. *J. Mater. Chem. A* **2018**, *6* (20), 9604−9612.
(39) Stoumpos, C. C.; Malliakas, C. D.; Kanatzidis, M. G. Semiconducting Tin and Lead Iodide Perovskites with Organic Cations: Phase Transitions, High Mobilities, and Near-Infrared Photoluminescent Properties. *Inorg. Chem.* **2013**, *52* (15), 9019−9038.
(40) Eperon, G. E.; Paternò, G. M.; Sutton, R. J.; Zampetti, A.; Haghighirad, A. A.; Cacialli, F.; Snaith, H. J. Inorganic Caesium Lead Iodide Perovskite Solar Cells. *J. Mater. Chem. A* **2015**, *3* (39), 19688−19695.
(41) Yi, C.; Luo, J.; Meloni, S.; Boziki, A.; Ashari-Astani, N.; Grätzel, C.; Zakeeruddin, S. M.; Röthlisberger, U.; Grätzel, M. Entropic Stabilization of Mixed A-Cation ABX_3 Metal Halide Perovskites for High Performance Perovskite Solar Cells. *Energy Environ. Sci.* **2016**, *9* (2), 656−662.
(42) deQuilettes, D. W.; Zhang, W.; Burlakov, V. M.; Graham, D. J.; Leijtens, T.; Osherov, A.; Bulović, V.; Snaith, H. J.; Ginger, D. S.; Stranks, S. D. Photo-Induced Halide Redistribution in Organic−Inorganic Perovskite Films. *Nat. Commun.* **2016**, *7* (1), 11683.
(43) Holovský, J.; Peter Amalathas, A.; Landová, L.; Dzurňák, B.; Conrad, B.; Ledinský, M.; Hájková, Z.; Pop-Georgievski, O.; Svoboda, J.; Yang, T. C.-J.; Jeangros, Q. Lead Halide Residue as a Source of Light-Induced Reversible Defects in Hybrid Perovskite Layers and Solar Cells. *ACS Energy Lett.* **2019**, *4* (12), 3011−3017.
(44) Marchezi, P. E.; Therézio, E. M.; Szostak, R.; Loureiro, H. C.; Bruening, K.; Gold-Parker, A.; Melo, M. A.; Tassone, C. J.; Tolentino, H. C. N.; Toney, M. F.; Nogueira, A. F. Degradation Mechanisms in Mixed-Cation and Mixed-Halide $Cs_xFA_{1-x}Pb(Br_yI_{1-y})_3$ Perovskite Films under Ambient Conditions. *J. Mater. Chem. A* **2020**, *8* (18), 9302−9312.
(45) Tang, X.; Brandl, M.; May, B.; Levchuk, I.; Hou, Y.; Richter, M.; Chen, H.; Chen, S.; Kahmann, S.; Osvet, A.; et al. Photoinduced Degradation of Methylammonium Lead Triiodide Perovskite Semiconductors. *J. Mater. Chem. A* **2016**, *4* (41), 15896−15903.
(46) Svanström, S.; Jacobsson, T. J.; Boschloo, G.; Johansson, E. M. J.; Rensmo, H.; Cappel, U. B. Degradation Mechanism of Silver Metal Deposited on Lead Halide Perovskites. *ACS Appl. Mater. Interfaces* **2020**, *12* (6), 7212−7221.
(47) Dastidar, S.; Hawley, C. J.; Dillon, A. D.; Gutierrez-Perez, A. D.; Spanier, J. E.; Fafarman, A. T. Quantitative Phase-Change Thermodynamics and Metastability of Perovskite-Phase Cesium Lead Iodide. *J. Phys. Chem. Lett.* **2017**, *8* (6), 1278−1282.
(48) Yuan, G.; Ritchie, C.; Ritter, M.; Murphy, S.; Gómez, D. E.; Mulvaney, P. The Degradation and Blinking of Single $CsPbI_3$ Perovskite Quantum Dots. *J. Phys. Chem. C* **2018**, *122* (25), 13407−13415.
(49) Li, N.; Luo, Y.; Chen, Z.; Niu, X.; Zhang, X.; Lu, J.; Kumar, R.; Jiang, J.; Liu, H.; Guo.; et al. Microscopic Degradation in Formamidinium-Cesium Lead Iodide Perovskite Solar Cells under Operational Stressors. *Joule* **2020**, *4* (8), 1743−1758.

https://dx.doi.org/10.1021/acsenergylett.0c02247
ACS Energy Lett. 2021, 6, 934−940